Available online at www.sciencedirect.com
SCIENCE DIRECT®
Journal of Applied Geophysics 54 (2003) 15–33
JOURNAL OF APPLIED GEOPHYSICS
www.elsevier.com/locate/jappgeo

Improving ground-penetrating radar data in sedimentary rocks using deterministic deconvolution

Jianghai Xia[a,*], Evan K. Franseen[a], Richard D. Miller[a], Thomas V. Weis[b], Alan P. Byrnes[a]

[a] *Kansas Geological Survey, The University of Kansas, 1930 Constant Avenue, Campus West, Lawrence, KS 66047-3726, USA*
[b] *Newmont Mining Corporation, 10101 East Dry Creek Road, Engewood, CO 80112, USA*

Received 29 August 2002; accepted 7 July 2003

Abstract

Resolution is key to confidently identifying unique geologic features using ground-penetrating radar (GPR) data. Source wavelet "ringing" (related to bandwidth) in a GPR section limits resolution because of wavelet interference, and can smear reflections in time and/or space. The resultant potential for misinterpretation limits the usefulness of GPR. Deconvolution offers the ability to compress the source wavelet and improve temporal resolution. Unlike statistical deconvolution, deterministic deconvolution is mathematically simple and stable while providing the highest possible resolution because it uses the source wavelet unique to the specific radar equipment. Source wavelets generated in, transmitted through and acquired from air allow successful application of deterministic approaches to wavelet suppression. We demonstrate the validity of using a source wavelet acquired in air as the operator for deterministic deconvolution in a field application using "400-MHz" antennas at a quarry site characterized by interbedded carbonates with shale partings. We collected GPR data on a bench adjacent to cleanly exposed quarry faces in which we placed conductive rods to provide conclusive groundtruth for this approach to deconvolution. The best deconvolution results, which are confirmed by the conductive rods for the 400-MHz antenna tests, were observed for wavelets acquired when the transmitter and receiver were separated by 0.3 m. Applying deterministic deconvolution to GPR data collected in sedimentary strata at our study site resulted in an improvement in resolution (50%) and improved spatial location (0.10–0.15 m) of geologic features compared to the same data processed without deterministic deconvolution. The effectiveness of deterministic deconvolution for increased resolution and spatial accuracy of specific geologic features is further demonstrated by comparing results of deconvolved data with nondeconvolved data acquired along a 30-m transect immediately adjacent to a fresh quarry face. The results at this site support using deterministic deconvolution, which incorporates the GPR instrument's unique source wavelet, as a standard part of routine GPR data processing.

Keywords: Ground-penetrating radar; Deterministic deconvolution; Stratigraphic studies

1. Introduction

Accurate interpretation of geologic features from ground-penetrating radar (GPR) data depends on data

* Corresponding author. Tel.: +1-785-864-2057; fax: +1-785-864-5317.
E-mail address: jxia@kgs.ku.edu (J. Xia).

0926-9851/$ - see front matter © 2003 Elsevier B.V. All rights reserved.
doi:10.1016/S0926-9851(03)00045-4

resolution. Ringing (related to bandwidth) in a GPR section as in seismic sections negatively impacts resolution and, therefore, must be identified and reduced or eliminated. Ignored ringing in radar limits the usefulness of GPR and increases the potential for misinterpretations. Deconvolution is essential to increasing the temporal resolution that is critical for shallow stratigraphic studies and allowing optimal interpretation of GPR data. A few studies have successfully applied a statistical approach to deconvolution of GPR data (Turner, 1992; Todoeschuck et al., 1992; Neves et al., 1995; Gottsche et al., 1994; Porsani and Ursin, 1996; Arcone et al., 1998; Moran et al., 2000). However, these deconvolution approaches are complicated in real-world sedimentary rock sites by multiple reflections not accounted for in statistical deconvolution approaches and assumptions inherent to most statistical deconvolution models (e.g., assuming reflectivity is a random process). We conducted a multiphase integrative study at a quarry

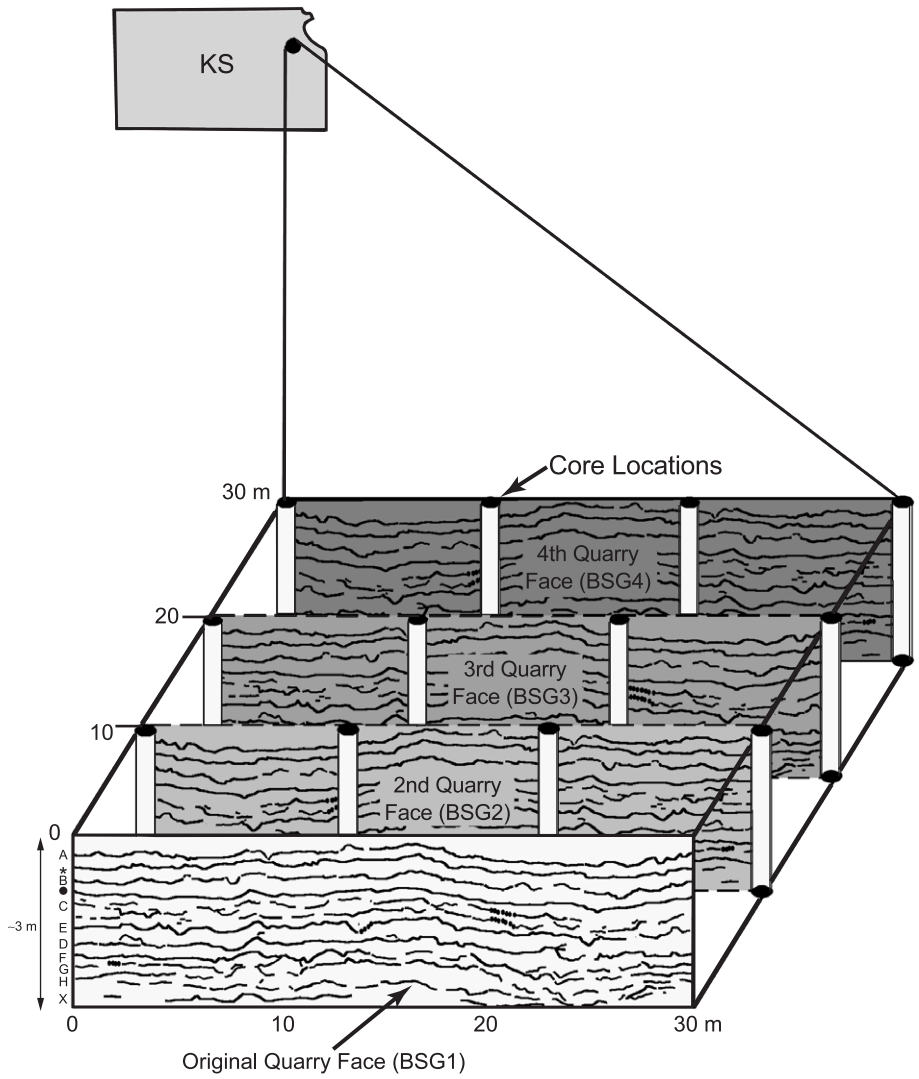

Fig. 1. Line drawing showing the 30 × 30-m two-dimensional grid on a flat bench behind an initial quarry face (BSG1) approximately 2.7–3.5 m (9–12 ft) thick. Successive quarry face exposures and 12 cores provided initial groundtruth for GPR interpretations.

site designed to address stratal, lithologic, petrophysical and geophysical properties influencing GPR responses. It became evident that we needed to develop new strategies and methods that improved the resolution and, therefore, use of GPR in shallow sedimentary rock studies. This paper focuses on a method designed to eliminate ringing effects in real-world GPR data using deterministic deconvolution (p. 93, Yilmaz, 1987). This form of deconvolution eliminates the assumptions inherent in statistical deconvolution approaches and results in data representing the earth's reflectivity series with minimal source wavelet effects.

Our study employed a convolution model using a GPR source wavelet propagated in the air. The convolution model was evaluated during deterministic deconvolution of GPR data acquired on a bench overlying Pennsylvanian carbonate and interbedded thin shale layers that were exposed in a quarry near Bonner Springs, KS (Fig. 1). We mapped geologic features on four successive quarry faces that were exposed during excavation and correlated those features with GPR data collected just behind the faces. We inserted conductive metal rods, 1.5 m in length, into horizontal drill holes placed in the quarry faces to provide easily identifiable signatures on GPR profiles and to serve as known reflecting/diffracting points (Xia et al., 2001; Franseen et al., 2001; Butler et al., 2000). The steel rods provide critical information for: (1) correlation between reflections on GPR data and geologic features exposed in the quarry face, (2) GPR resolution limits, (3) accuracy of velocities calculated from common midpoint (CMP) data and (4) identifying multiples. Our results have significant ramifications to both improving the quality of GPR data and interpreting stratigraphy from GPR sections where successful suppression of wavelet effects is critical.

Although deconvolution has been utilized in the GPR industry for many years, it has not been effective in many situations. In our study, the interpretation of GPR data was improved after applying deterministic deconvolution using the source wavelet acquired in air at a field study site composed predominantly of carbonate strata. We hope our initial study is a positive contribution to the application of deterministic deconvolution for GPR stratigraphic studies of low dielectric loss media, such as carbonate strata.

2. Deconvolution

Deconvolution is a numerical process that compresses the basic source wavelet, thereby improving temporal resolution. There are many different deconvolution methods that have been applied to seismic reflection data (Yilmaz, 1987). Deconvolution has also been applied to GPR data in hopes of improving resolution in a fashion consistent with its use on conventional seismic reflection data. Different methods of deconvolution applied to GPR data include: propagation deconvolution (Turner, 1992, 1994), predictive deconvolution (Todoeschuck et al., 1992), two-sided deconvolution (Gottsche et al., 1994), mixed-phase deconvolution (Porsani and Ursin, 1996) and source signature deconvolution (Neves et al., 1995). Recently, a Wiener deconvolution filter (Yilmaz, 1987) successfully broadened the wavelet bandwidth, thereby improving the temporal resolution of GPR data (Moran et al., 2000). All of these deconvolution methods require assumptions be made about the source wavelet and/or the extraction of the source wavelet from GPR data using a statistically determined method.

Spiking deconvolution is another approach that assumes the earth reflectivity is a random process and the spectrum of the source wavelet has no zeros (Yilmaz, 1987). However, the bandwidth and signal-to-noise characteristics of GPR data and the limited number of layers in the near surface violate the basic assumptions of spiking deconvolution.

As an alternative to statistically based methods, deterministic deconvolution (p. 93, Yilmaz, 1987) is numerically the simplest and most stable of all types of deconvolution and is equivalent to spiking deconvolution when an source wavelet, the pulse emitted from a GPR transmitter antenna, is available. In the next section, we further describe how we applied deterministic deconvolution to improve GPR data.

3. Deterministic deconvolution

Assuming no noise, GPR data are the convolution of the source wavelet with the earth's reflectivity series such that:

$$x(t) = w(t)*e(t), \quad (1)$$

where $x(t)$ is the recorded GPR trace, $w(t)$ is the source wavelet, $e(t)$ is the earth's reflectivity series or impulse response and * denotes convolution. If the source wavelet is known, the solution to the deconvolution problem (1) is called deterministic deconvolution (p. 93, Yilmaz, 1987).

The simple convolution model (Eq. (1)) relies on the fact that the source wavelet does not change either from place to place or as a function of antenna–ground coupling. Antenna ground coupling and EM energy propagating in the earth produce additional wavelets $u(t)$ other than the source wavelet. The convolution model in this case simply replaces the source wavelet $w(t)$ with $s(t)$*$u(t)$ (Eq. (2.31), p. 133, Yilmaz, 1987) in Eq. (1), where convolution of $u(t)$, the unknown wavelet with $s(t)$, the source wavelet is equivalent to $w(t)$ in Eq. (1). The unknown wavelet $u(t)$ includes the propagating effects in the earth and the response of the recording system. Effects of this unknown wavelet become significant in high dielectric loss media such as wet soil. Acquisition of this wavelet is difficult and site dependent. It requires statistical methods to remove this unknown wavelet (e.g., Turner, 1994; Todoeschuck et al., 1992; Gottsche et al., 1994; Porsani and Ursin, 1996). When GPR data are acquired in low dielectric loss media, such as snow, or the carbonate strata at our testing site, effects of the unknown wavelet may be negligible as our examples demonstrate in the following sections. In all cases, however, removal of the source wavelet $s(t)$ by the deterministic deconvolution has the potential to provide the highest possible resolution independent of data characteristics. Therefore, in the following discussion, we assume the effect of the unknown wavelet $u(t)$ can be ignored.

In the frequency domain, Eq. (1) can be written as:

$$X(f) = W(f)E(f), \tag{2}$$

where $X(f)$ is the Fourier transform of $x(t)$, $W(f)$ is the Fourier transform of $w(t)$ and $E(f)$ is the Fourier transform of $e(t)$.

If $W(f)$ does not go to zero within a specific range, an earth reflectivity series can be determined using a deterministic deconvolution

$$E(f) = X(f)/W(f) \tag{3}$$

and the inverse Fourier transform

$$e(t) = F^{-1}[E(f)] \tag{4}$$

where F^{-1} is the inverse Fourier transform.

If $W(f)$ possesses zeros in its spectra within a frequency range of interests, we could apply Claerbout's (1992, p. 86) suggestion that multiplies the numerator and denominator terms of Eq. (3) by the complex conjugate $\overline{W(f)}$ and adds a damping factor ε^2 to the denominator. Thus, Eq. (3) becomes

$$E(f) = \frac{X(f)\overline{W(f)}}{W(f)\overline{W(f)} + \varepsilon^2}. \tag{3}*$$

The denominator is always a positive number greater than zero, so division is safe. Claerbout (1992, p. 86) also discussed a practical way to choose the damping factor.

Tests on synthetic GPR data showed obvious differences between the deterministic deconvolution and the predictive deconvolution. To generate synthetic data, we measured matrix composition to establish component dielectric constants and measured dielectric constants at a centimeter scale from rock material collected at the test site (Fig. 1). Component dielectric constants for the minerals, water, air, and relative concentrations were used to calculate bulk dielectric constants using the Time Propagation model (Knoll, 1996) that has been previously shown to accurately predict bulk properties for these lithologies at our study sites (Martinez and Byrnes, 2001). A reflectivity model (Fig. 2a) was generated solely from the bulk dielectric constants. Synthetic GPR reflection data (Fig. 2b) were produced using the convolution model (Eq. (1)). Deterministic deconvolution was applied to the synthetic data (Fig. 2c). The reflectivity series was recovered (except for a scaling factor) as expected because the source wavelet is known. Predictive deconvolution was also applied to the synthetic data with different predictive lags (from 1.5 to 6 ns). A filter length of 6 ns was chosen to be consistent with the length of the source wavelet. The best results after the predictive deconvolution (a predictive lag of 3 ns) are shown in Fig. 2d. Because the predictive deconvolution estimates the source wavelet based on the assumption that reflectivity is a

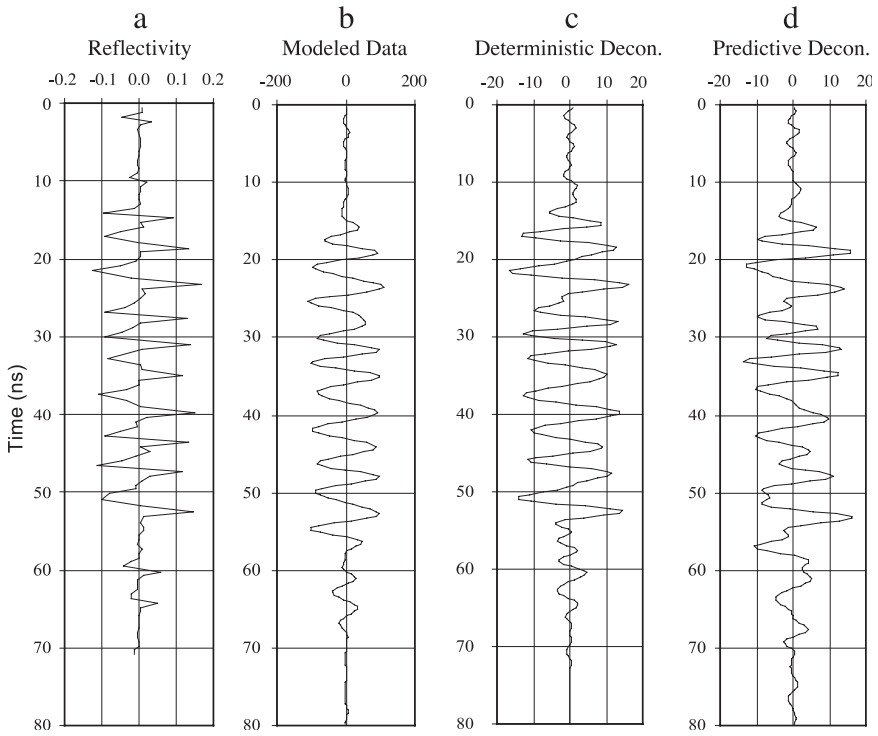

Fig. 2. Reflectivity model and synthetic GPR traces. The reflectivity model (a) was generated from bulk dielectric constants. The synthetic GPR reflection data (b) were calculated from the reflectivity model using the convolution model. Traces after the deterministic deconvolution (c) and the predictive deconvolution (d) are shown for comparison.

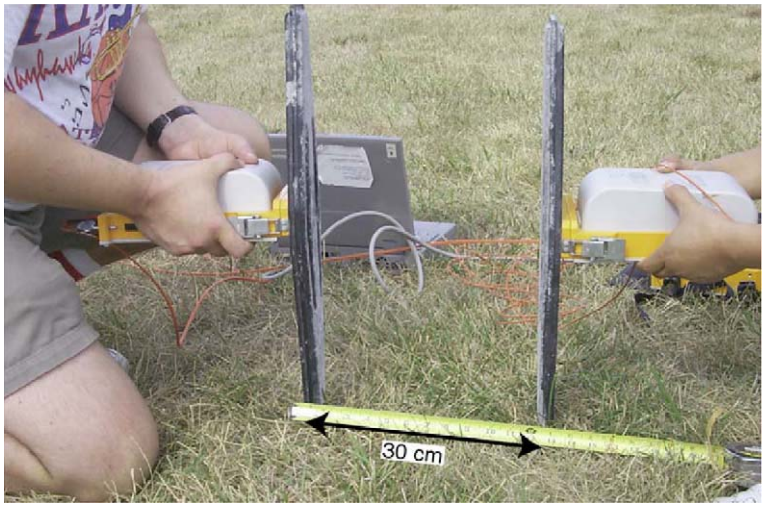

Fig. 3. Both antennas of the MALÅ RAMAC system were placed face to face to acquire wavelets in the air.

random process (Yilmaz, 1987), predictive deconvolution was not as effective and the recovered reflectivity series was not as accurate in comparison with the deterministic deconvolution where the source wavelet is known.

Since wavelets acquired in the air are true source wavelets, changes in geologic setting have no impact on the convolution model used by the deterministic deconvolution operation. Therefore, once a representative wavelet is cataloged for each antenna, that wavelet can be used in all geologic settings and for all applications until the antenna is physically altered or electronically modified. In the next section, we will describe acquisition of the GPR source wavelet, which is the basis of the deterministic deconvolution.

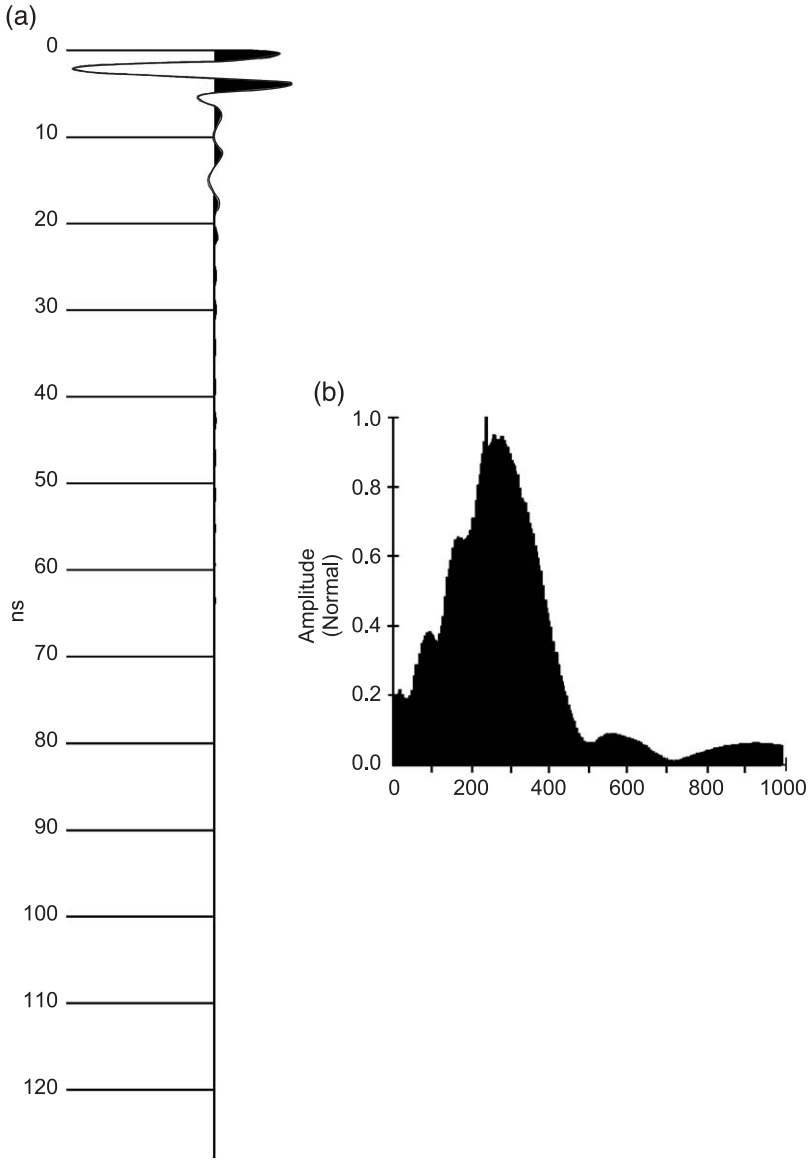

Fig. 4. (a) The wavelet of the 400-MHz antennas with 0.3 m separation in wavelet acquisition and (b) its spectrum.

4. Wavelet acquisition

We acquired GPR data for this study by using a MALÅ RAMAC system with a 370-V transmitter and 400-MHz antennas (producing 300-MHz signals). We processed the data using WinSeis© (a commercial software package developed at the Kansas Geological Survey) complemented with some custom code.

Acquisition of a clean source wavelet is critical to the effectiveness of deterministic deconvolution. Source wavelets were acquired in an open field that was void of environmental and/or cultural noise. The source wavelets were acquired by placing the antennas face to face with a separation of 0.3 m (Fig. 3). The main assumption in acquiring the source wavelet shown in Fig. 3 is that reflection energy from the grass surface is very weak relative to energy of the direct wave. This assumption is proved to be valid by steel rod tests shown in the following sections. A 512-fold vertical stack minimized the contribution of random noise during the acquisition of a representative wavelet. Empirical determination of the optimum wavelet for the MALÅ RAMAC instrument was accomplished through repetitive applications of deterministic deconvolution to a test data set using source wavelets recorded at each unique offset while the antennas were face to face. For example, the wavelet extracted with 0.3-m separation in wavelet acquisition produced the best deconvolution results for 400-MHz antennas. The well-behaved spectrum of the 400-MHz antenna wavelet (no zero or near-zero values in the spectrum) and a dominant frequency of 300 MHz (Fig. 4) allowed direct and stable application of deterministic deconvolution (Eq. (3)) to GPR data. We noticed there is some reverberation after the initial event (Fig. 4a). Wavelets acquired at separations of 0.6 and 0.9 m possess weaker reverberation as the separation increased indicating that the reverberation is likely caused by the relatively close proximity of the two antennas to one another.

Since the length of the wavelet from the 400-MHz antenna (Fig. 4a) is 5–6 ns, any reflected events with time duration equal to or longer than the length of the wavelet will interfere with each other, therefore, reducing resolution of GPR data. Study at a real-world stratigraphic site verifies that once the source wavelet has been removed (Fig. 4a) from the GPR data by deterministic deconvolution, temporal resolution will increase and the true position of reflections can be more accurately determined.

5. Verification of deterministic deconvolution from the study site

We used exposures of Pennsylvanian carbonate strata from the upper Farley Member in the Shawnee

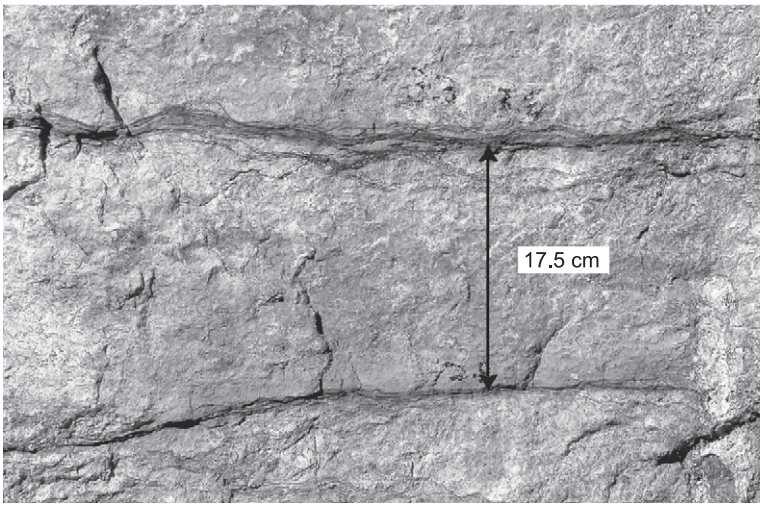

Fig. 5. Thin shale partings and stylocumulates that typically occur at carbonate bedding planes and reflect GPR signals. The shale partings are commonly diffused into adjacent carbonate over the scale of 0.5 to ~ 7.5 cm. Distance between shale layers on photo is 17.5 cm.

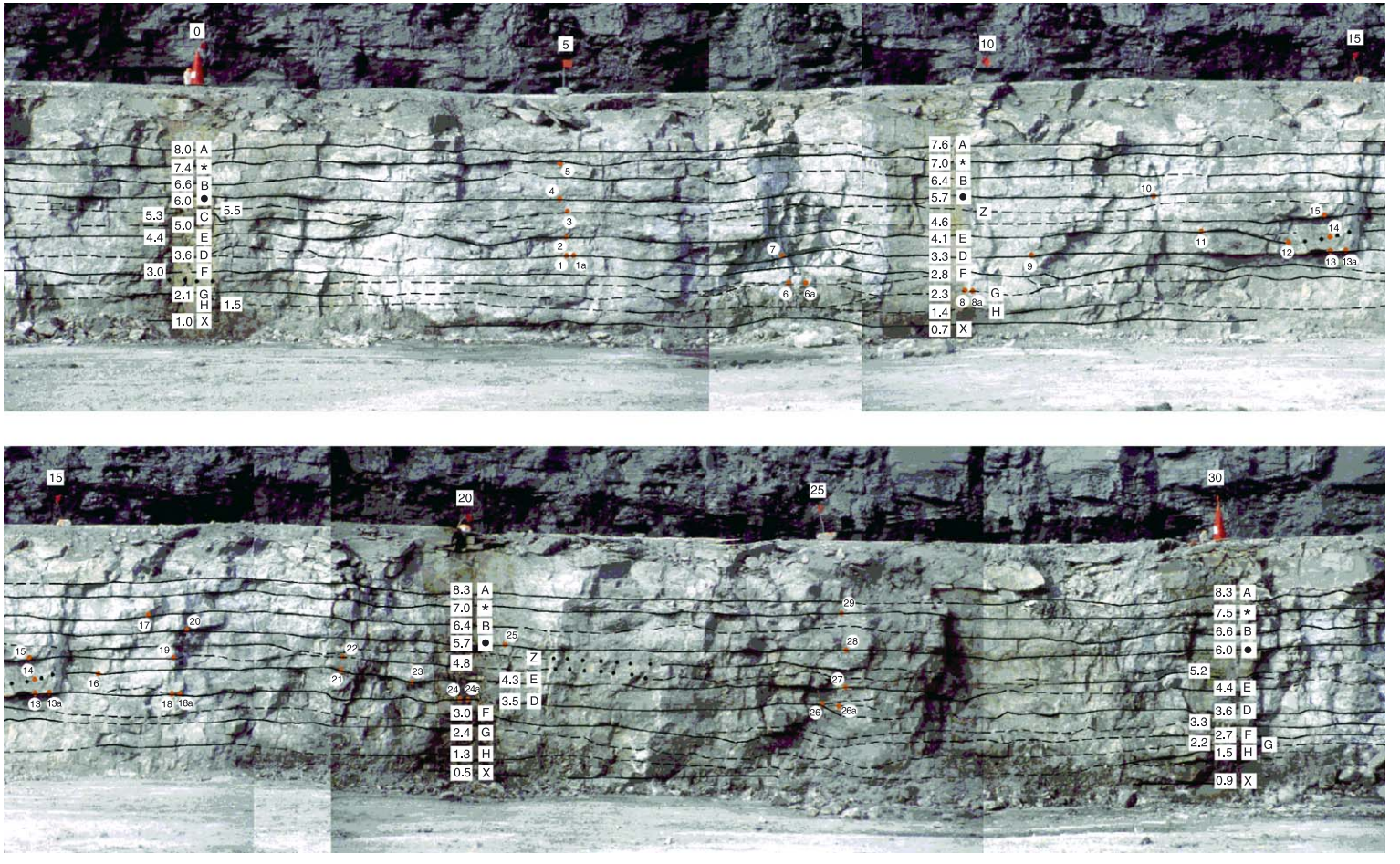

Fig. 6. Outcrop photomosaic showing nature of carbonate bedding and shale partings on the first quarry face (BSG1). Numbers at bedding horizons show scale in feet as measured vertically from quarry floor. Numbers along the top of quarry face are distances in meters. Letters and symbols are assigned to beds to facilitate comparison between the outcrop and results of GPR data. Orange dots and associated numbers show locations for horizontal conductive rod experiments.

Rock quarry near Bonner Springs, KS, to demonstrate the effectiveness of applying deterministic deconvolution for improved temporal and spatial resolution of GPR data. These strata are vertically exposed for approximately 3 meters on the quarry face and characterized by medium (<0.15 m) to thick (0.3–0.9 m) beds of limestone separated by thin (<2.5 cm) shale partings and stylocumulates (material that passively accumulated as insoluble residue along a pressure–solution surface) (Fig. 5). The shale partings and stylocumulates commonly diffuse into adjacent limestone over a scale of 0.5 to ~7.5 cm. The carbonate beds are composed of well-cemented skeletal wackestone and packstone consisting predominantly of phylloid algae, bryozoans, brachiopods and, locally, algal-coated grains (*Osagia*) in a matrix of micrite, peloidal micrite and microspar. They are interpreted to have been deposited in low- to moderate-energy marine environments (McKirahan et al., 2000). A characteristic of upper Farley strata is the lateral continuity of the generally horizontal bedding. Shale partings and stylocumulates at bedding planes are generally laterally consistent, but may be absent locally (Fig. 6).

We initially collected GPR data on a flat bench immediately behind a quarry face (BSG1) along a two-dimensional grid 30 × 30 m (Fig. 1). We profiled seven lines parallel to the quarry face and seven lines perpendicular to the quarry face, each separated by 5 m and recorded GPR data using 50-, 100-, 200- and 400-MHz antennas. We acquired a 128-fold vertical stack every 0.1 m along each line with the 400-MHz antennas while maintaining a fixed source and receiver separation of 0.6 m. A perpendicular-broadside antenna orientation was employed to give the radar section more of a two-dimensional slice through the subsurface (Annan, 1996).

Initial groundtruthing of GPR data was accomplished by mapping geologic features exposed as quarry operators blasted back at 10-m intervals in coordination with our three-dimensional grid and borehole (core) locations (Figs. 1 and 6). We inserted steel rods 1.5 m in length and 4.4 cm in diameter into holes drilled horizontally into the quarry face to provide direct groundtruth. A total of 78 horizontal holes were located at key spots on three exposed quarry faces, BSG1, BSG2 and BSG3 (Fig. 1).

A specially designed horizontal air-drilling unit provided holes with tolerances that required the rods to be driven snuggly into place. GPR data were acquired with a perpendicular broadside antenna orientation (the polarization of the antennas being parallel to the conductive steel rods) before and after the rods were placed in the holes. Reflections/diffractions from the rods on GPR data provided the exact locations of the subsurface being imaged, which, through comparisons to the measured rod locations in the quarry face, provide exact correlation of reflections to reflectors. For the purpose of this paper, focus is placed on the results of several experiments conducted on the initial (BSG1) and third quarry faces (BSG3).

5.1. GPR response from steel rods

One experiment measured the response of six vertically aligned steel rods in quarry face BSG3 (Table 1 and Fig. 7a). Time to depth conversions are based on EM wave propagation velocities calculated from moveout curves on the CMP data. We acquired GPR data along a 6-m line, 1 m behind the quarry face containing the steel rods. The conductive rods appear as hyperbolas on GPR data. Although the apex of the hyperbolas should indicate the precise location of the rods, the locations (horizontal and vertical) of the apexes of the hyperbola on the trapezoidal bandpass filtered (80/130–400/500 MHz) and automatic gain control scaled (AGC, a 10-ns window) GPR data are apparently skewed compared to the true rod locations (Fig. 7b). The average velocity of EM wave propagation in the carbonate at this site is 0.1 m/ns, which for the 400-MHz antenna equates to a maximum potential vertical resolution of around 0.25–0.30 m (Fig. 4a). Theoretically, two reflectors closer than 0.25–0.30 m will not be resolvable. With this limitation in resolution, the six rods on the nondeconvolved GPR data can only be located within a confidence of 0.1 m vertically and 0.2 m horizontally (Fig. 7b).

Table 1
Locations of horizontal rods

Number of hole	Horizontal (m)	Vertical (m)
1	31.46	0.732
2	31.34	1.113
3	31.63	1.387
4	31.46	1.875
5	31.34	2.103
6	31.46	2.271

In contrast, after including deterministic deconvolution in the processing, which consists of the deterministic deconvolution, trapezoidal bandpass filtering (80/130–400/500 MHz) and AGC (a 10-ns window), the apexes of the four shallowest hyperbolas distinctly and correctly represent the locations of the corresponding four rods both horizontally and vertically (Fig. 7c). The reason behind selecting the parameters of the trapezoidal bandpass filter is to keep energy around the dominant frequency (300 MHz) and eliminate noise energy generated by the deterministic deconvolution. Using a normal moveout velocity calculated from a nearby CMP gather (0.097 m/ns), the true depths of the first four rods can be located within a few centimeters from the GPR data. It is also now possible to locate the two deepest rods (numbers 5 and 6) even though conventional wisdom would suggest they are too deep to detect (considering their size and penetration limitations for antennas of this frequency) and not uniquely detectable since they are separated by

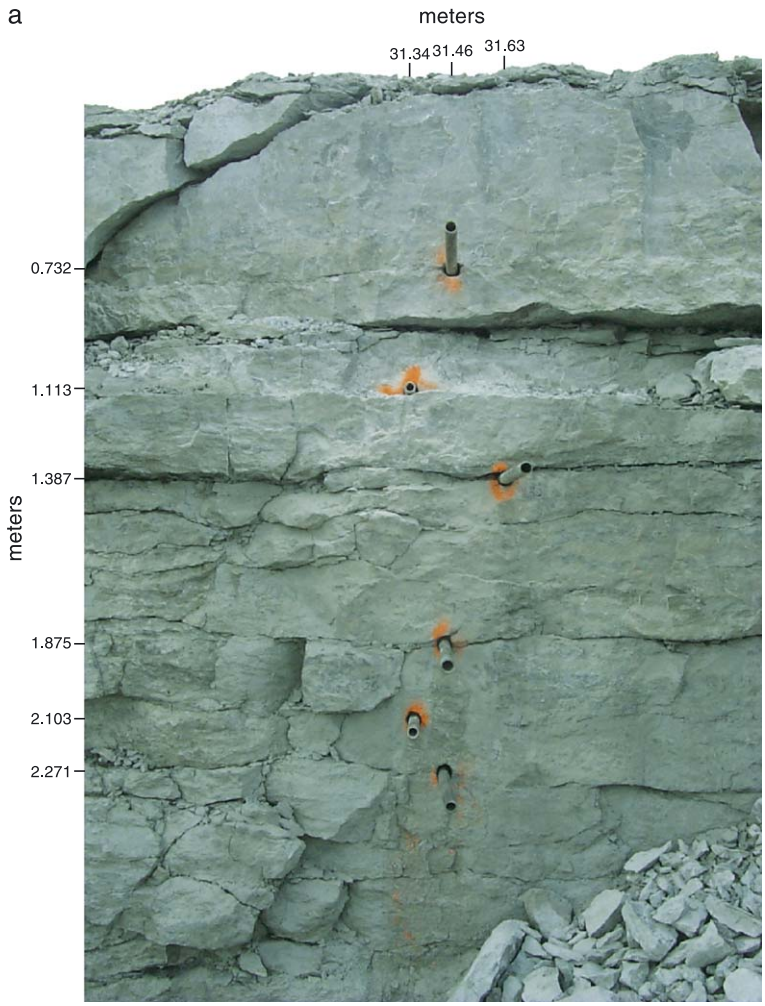

Fig. 7. (a) Outcrop photo of part of quarry face BSG3 containing six horizontal holes with steel rods. (b) The 400-MHz GPR data, trapezoidal bandpass (80/130–400/500 MHz) filtered and scaled (10-ns AGC) along a 6-m line on the bench 1 m behind the quarry face. (c) GPR data after the deterministic deconvolution, the trapezoidal bandpass filtering and the AGC. (d) GPR data after the AGC. (e) GPR data after the deterministic deconvolution and the AGC. (f) GPR data after spherical/exponential gain (velocity = 0.1 m/ns and $\alpha = 0.01$ dB/m). (g) GPR data after the deterministic deconvolution and the spherical/exponential gain. Open dots in (b)–(g) represent rod locations as shown on (a).

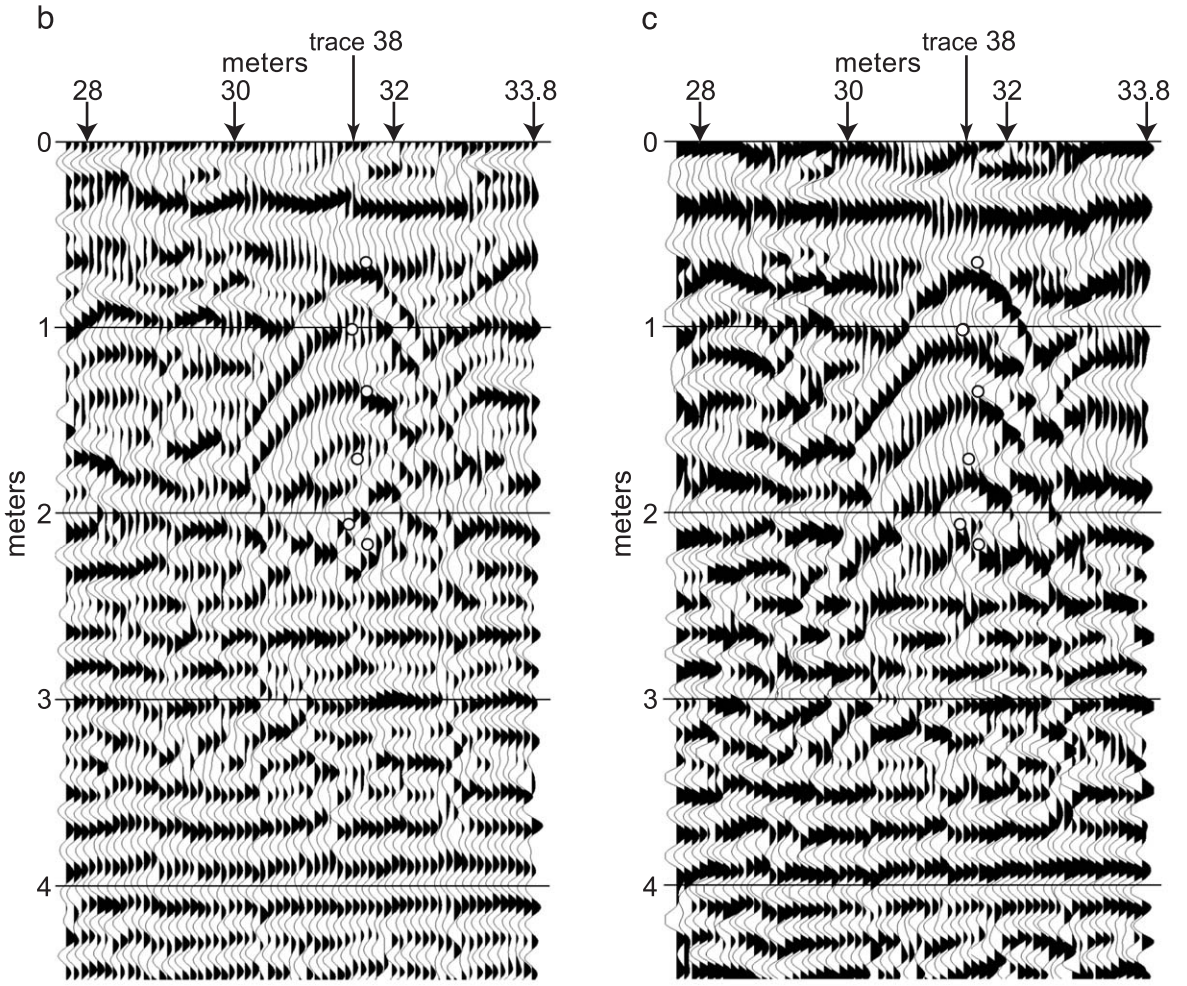

Fig. 7 (*continued*).

less than one-quarter wavelength. The spectra of Fig. 7b and c appear the same visually. This is because we applied the same trapezoidal bandpass filter (80/130–400/500 MHz) to data both with and without the deterministic deconvolution.

To eliminate effects from the trapezoidal bandpass filter, Fig. 7d and e show results without the trapezoidal bandpass filter. Only AGC (a 10-ns window) was applied for Fig. 7d and the deterministic deconvolution (to flat the spectra up to 800 MHz) and AGC (a 10-ns window) were applied for Fig. 7e. Results after the deterministic deconvolution show clearer images of the steel rods.

We also evaluated the possibility of waveform changes due to AGC processing. Only Spherical/Exponential Gain (velocity = 0.1 m/ns, $\alpha = 0.01$ dB/m) was applied for Fig. 7f. Deterministic deconvolution (to flatten the spectra up to 800 MHz) and the Spherical/Exponential Gain were applied for Fig. 7g. Fig. 7c, e and g and the results indicate that the improvement of the images is due to the deterministic deconvolution.

The improvement in resolution after deterministic deconvolution is further demonstrated using a single ray trace (Fig. 8) (trace 38 from the GPR data in Fig. 7). The shallowest five rods, labeled as 1, 2, 3, 4 and 5, clearly correlate to negative peaks after using deter-

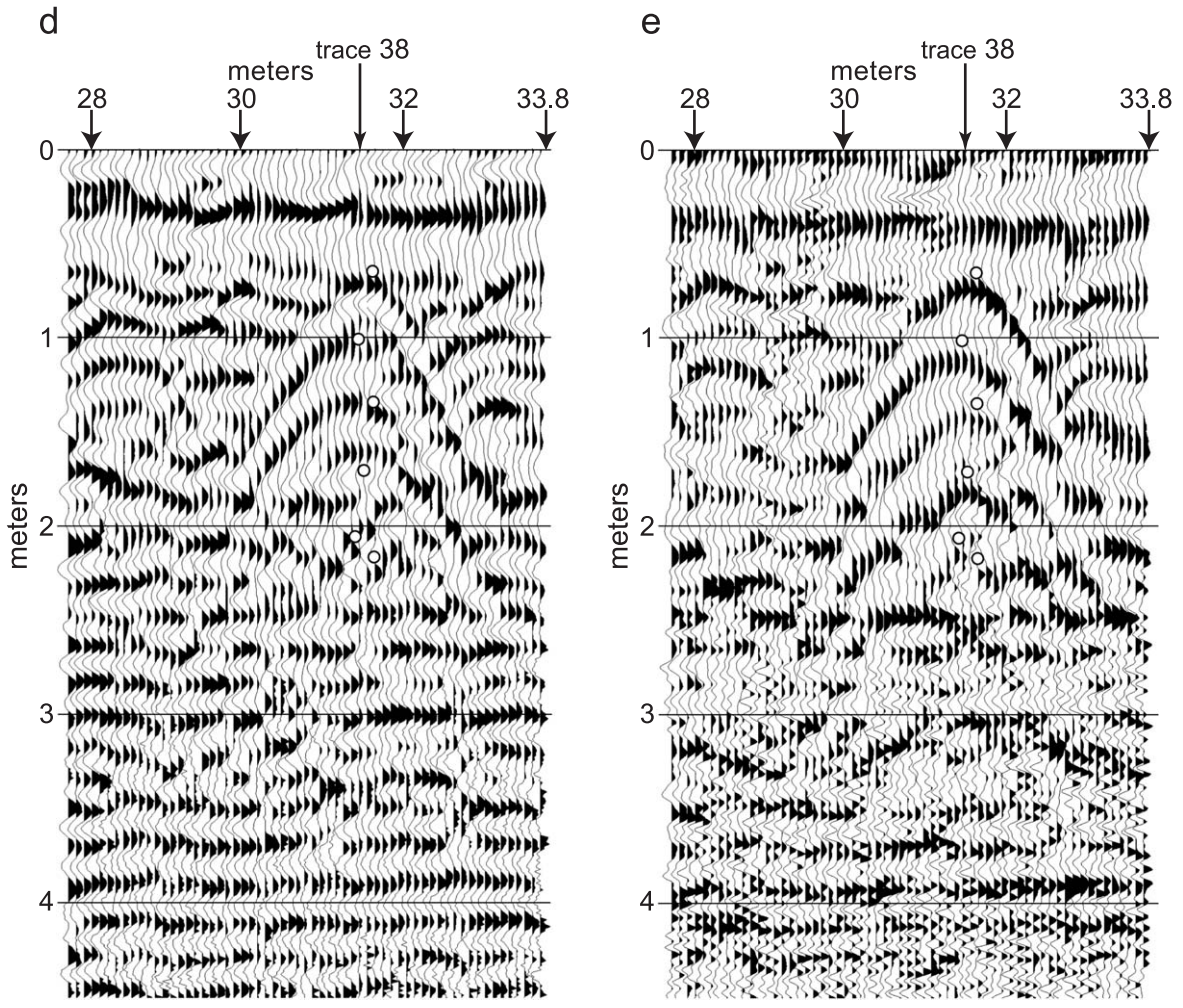

Fig. 7 (*continued*).

ministic deconvolution (Fig. 8b). Only the deepest rod (6) is not confidently correlated to a negative peak. In comparison, we were not able to confidently identify any of the six rods on the nondeconvolved GPR data (Fig. 8a).

In another experiment, we placed 10 steel rods laterally along the BSG1 face at the bed E and bed D horizons (Figs. 6 and 9). GPR data were again acquired along a line 1 m behind the quarry face. Some reflections on only trapezoidal bandpass filtered (80/130–400/500 MHz) and scaled (10-ns AGC) GPR data (Fig. 9a) appear to correlate with the stratigraphy shown on the photomosaic; however, much of the GPR data are very difficult to interpret due to the dominance of a very complex arrival pattern characteristic of wavelet interference, and possible out-of-plane energy. Based on the results of the first steel rod experiment discussed earlier, many of these complexities are due to lower data resolution and associated wavelet interference, making it difficult to interpret most of the bedding on this section. The locations of the 10 rods are labeled based on field spatial measurements (Fig. 9). Due to the limited temporal resolution of nondeconvolved GPR data (Fig. 9a), locations of some of the 10 horizontal steel rods on beds E and D of the BSG1 face cannot be confidently determined.

Resolution of the GPR image is considerably increased after the deterministic deconvolution, trap-

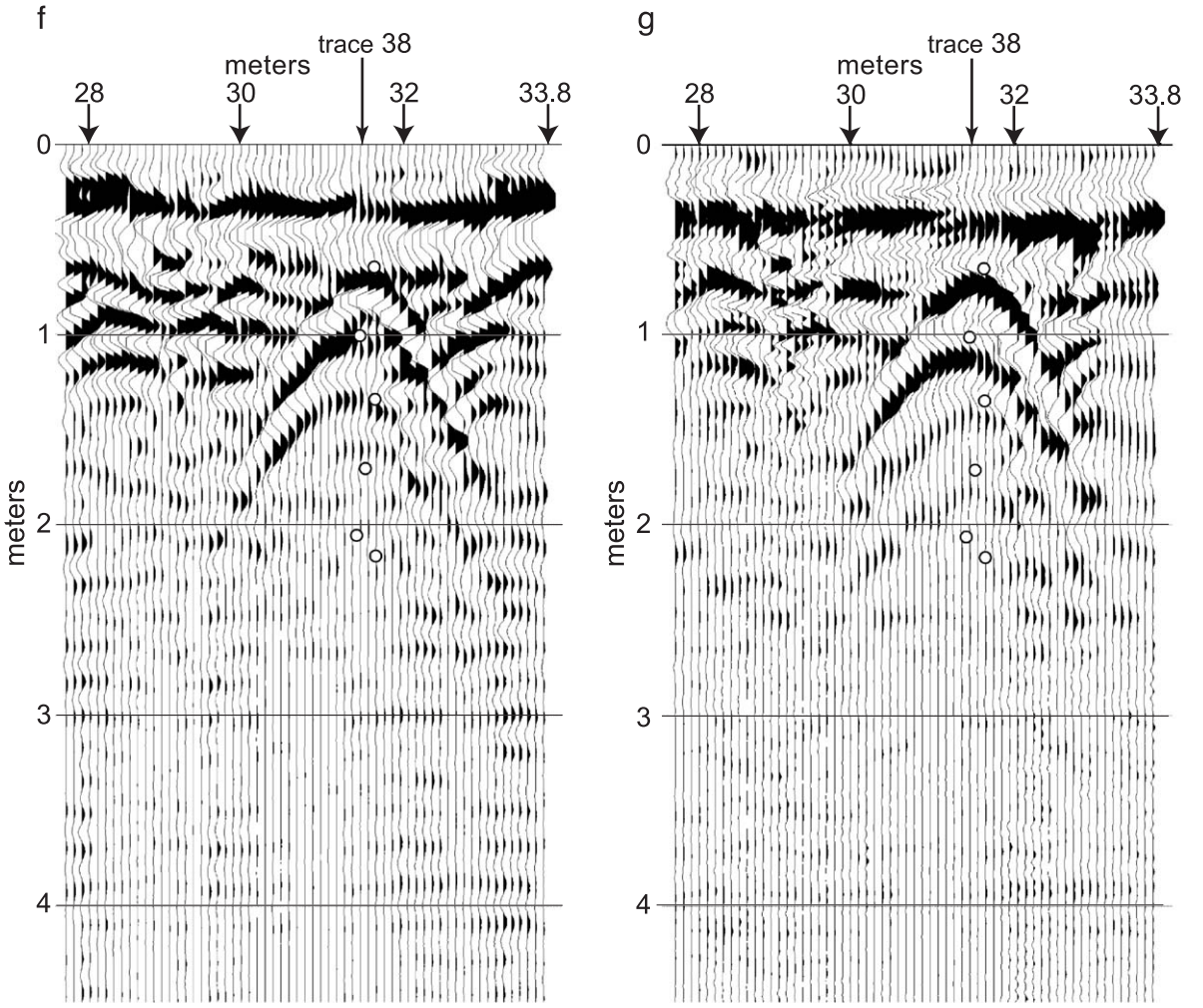

Fig. 7 (*continued*).

ezoidal bandpass filtering (80/130–400/500 MHz) and scaling (10-ns AGC) (Fig. 9b). The direct benefit from the deterministic deconvolution is that the wavelet ringing is subdued, which is clearly indicated by diffractions from rods 7, 9, 11, 12 and 27. Diffractions from the rods in the deconvolved data are clearly identified and indicate: (1) reflection events are from specific geologic features, exemplified by clear reflection events at the E and D horizons along the entire trace, and (2) the locations of geologic features are spatially accurate. Beds E and D along the BSG1 face are spatially accurate along the entire deconvolved GPR trace as confirmed by measurements from the quarry face. Reflections from the steel rods confirm that reflection events on the GPR data are primary reflections and not multiples.

Images from all rod tests (Figs. 7 and 9) place the reflectors and the steel rods at their spatially correct locations (based on observations and measurements on the quarry face) with representative amplitudes after the deterministic deconvolution with the wavelet acquired at a separation of 0.3 m. This is the basis for suggesting "optimal results" were obtained using a separation of 0.3 m.

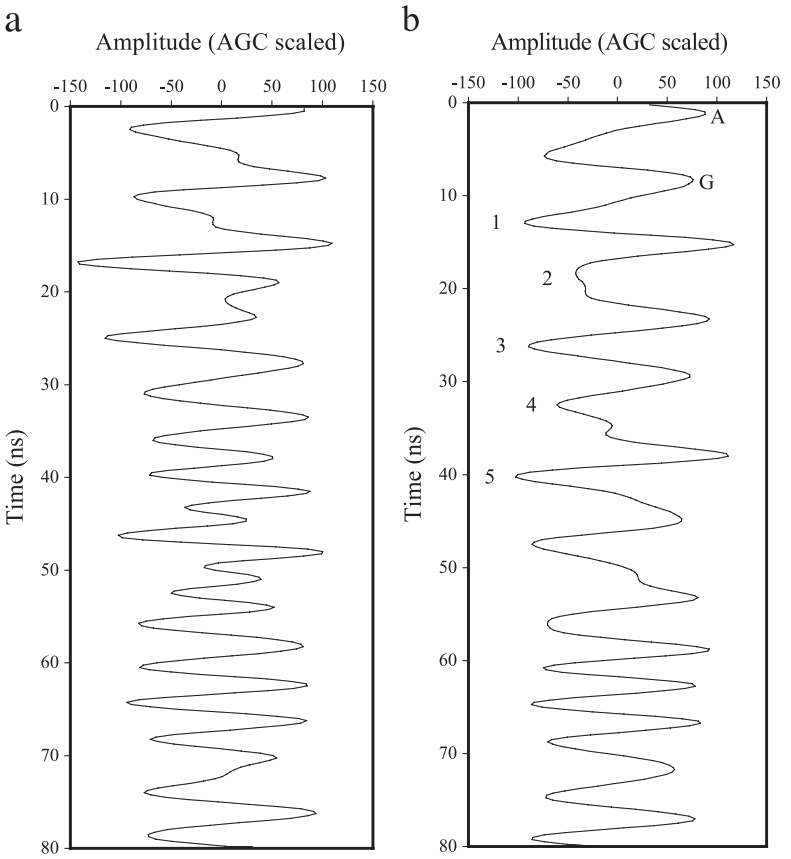

Fig. 8. Trace 38 from Fig. 7b (a) and Fig. 7c (b). After the deterministic deconvolution, the negative peaks of the trace (b) labeled 1–5 correspond with steel rods 1–5 correctly. The air wave and the ground wave are labeled as A and G (b), respectively. These relationships are not clear in the trace before deterministic deconvolution (a).

We noticed that some diffractors from the steel rods (e.g., rod 7 in Fig. 9b) seem to show flipped polarity. However, reflectors from horizons just below the rod (at 3-m depth) do not show flipped polarity. Because the processing steps that we used only include the deterministic deconvolution, trapezoidal bandpass filtering (80/130–400/500 MHz), and AGC (a 10-ns window), we believe the shape of the wavelet change is solely due to the deterministic deconvolution because the source wavelet is compressed.

5.2. Comparing geologic features with GPR images along a quarry face: an example of improved stratigraphic interpretation using deterministic deconvolution

This section further demonstrates the usefulness of deterministically deconvolved data to improve resolution by directly comparing geologic features mapped along the face of a 30-m segment of quarry exposure with deconvolved and nondeconvolved GPR data.

Fig. 9. Profile over 10 steel rods drilled into beds E and D. Two rods (numbers 2 and 3 from the left) were on bed D and the rest on bed E. (a) GPR data produced with 400-MHz antennas along a 30-m line on a flat bench 1 m behind quarry face BSG1 after trapezoidal bandpass filtering (80/130–400/500 MHz) and AGC (a 10-ns window) have been applied. (b) The same GPR data as shown in (a) after the deterministic deconvolution, the trapezoidal bandpass filtering and the AGC. Open dots indicate the locations of steel rods.

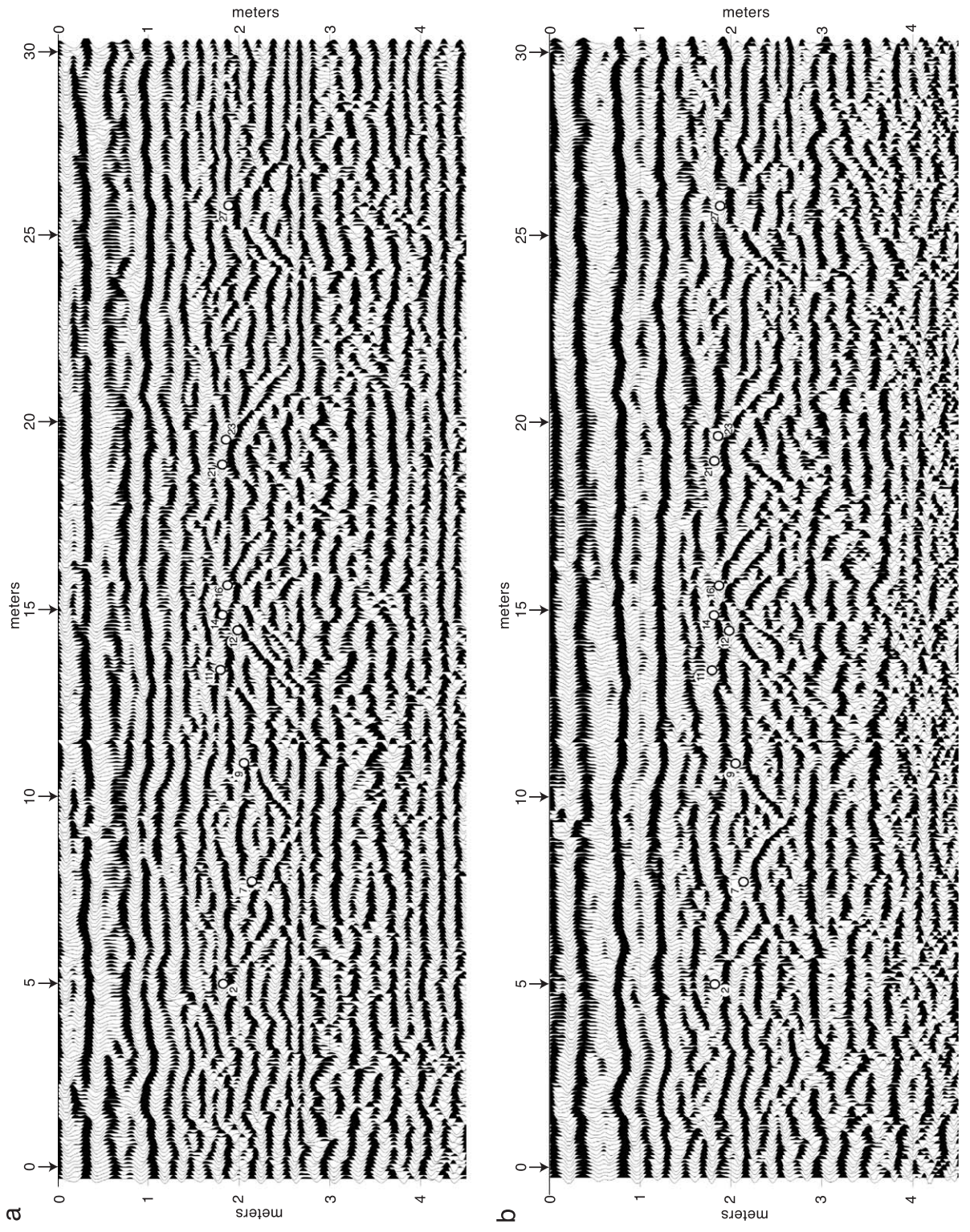
a
b
meters
meters
meters
meters

Lines drawn on a photomosaic of the quarry face show the bedding characteristics of the carbonates and shales (Fig. 6). Solid lines represent distinct, traceable bedding planes (shale partings), dashed lines reflect less distinct bedding planes (shale partings are thinner or more diffuse) and dotted lines represent nondistinct, inferred bedding planes (absence of shale). Letters and symbols are assigned to beds to facilitate comparison between the outcrop and GPR data. Edge effects due to the quarry face were not evident on the profile even though it was taken only 1 m behind the quarry face. This observation was made after comparing two GPR data sets acquired along the same line before and after the blasting of successive quarry faces (Xia et al., 2001).

Due to the limited temporal resolution of nondeconvolved GPR data (Fig. 10a), locations of some of the 32 horizontal steel rods (not marked) on the BSG1 face cannot be confidently determined.

As we mentioned earlier in this paper, the maximum potential vertical resolution is around 0.25–0.30 m for data at this site. Because GPR data after deterministic deconvolution (Fig. 10b) clearly defined beds that are about 0.18 m thick (top three beds) and 0.15 m thick (the bed between D and F under the 10-m mark), resolution of the GPR image appears to have increased by at least 50%.

Time to depth conversions (Fig. 10) are based on EM wave propagation velocities calculated from moveout curves on the CMP data. Accuracy of these conversions was confirmed by comparing surveyed horizontal rod locations along the BSG1 face with depths calculated from GPR data. This ultimate groundtruthing (surveyed conductive rods driven into the quarry face) confirms that the deterministic deconvolution approach to processing GPR data improves the resolution of GPR data.

A comparison between some general characteristics of the documented quarry face (Fig. 6) with the deconvolved data (Fig. 9b) and then with the only trapezoidal bandpass filtered (80/130–400/500 MHz) and scaled (10-ns AGC) data (Fig. 10a) further highlights the effectiveness of the deterministic deconvolution. Beds *, ·, E, and X are distinct, laterally traceable beds with bedding planes characterized by relatively thick shale partings (Fig. 6). Consistent with reflectivity estimations, these horizons should be, and are, strong, laterally continuous reflections on deconvolved GPR data (Fig. 10b). However, these horizons are neither distinctly identifiable nor laterally continuous on nondeconvolved data (Fig. 10a).

Beds A and B are distinct, laterally traceable horizons on BSG1 quarry exposures, with bedding planes characterized by lateral variations in shale concentration. Based on the lateral variations in shale concentration, the GPR image of beds would be expected to possess some variability in reflection wavelet character as a function of the differing shale concentrations. On deconvolved data, which go through the deterministic deconvolution, trapezoidal bandpass filtering (80/130–400/500 MHz) and scaling (10-ns AGC), beds A and B are confidently identified and, as expected, their reflection character varies laterally (Fig. 10b). Identification of beds A and B on nondeconvolved data is more complicated and requires identification of the more distinct * and · beds to use as a guide. However, the * and · beds are also a challenge to identify on nondeconvolved sections (Fig. 10a).

Beds F, G and H are distinct horizons that are traceable with varying degrees of confidence along the BSG1 quarry face. These beds are geologically characterized by lateral variability in bedding plane shale amounts and pinching and swelling geometries. Therefore, reflection characteristics of these horizons on GPR data should include laterally variable reflection amplitudes and geometric complexities. The general locations of beds F, G and H can be confidently located on the deconvolved section when aided by location of the more distinct laterally continuous E and X bedding horizons (Fig. 10b). As expected from mapping of the quarry face, beds F, G and H possess lateral variation in reflection character and geometric complexity on deconvolved data (Fig. 10b). In contrast, locations of beds F, G and H are virtually impossible to confidently locate on nondeconvolved data due to overall complexity associated with wavelet interference and noise on GPR data at those depths (Fig. 10a).

Finally, the beds between the E and · beds (including Z, C and several unlabelled beds) are the most difficult to trace in outcrop due to bedding planes that die out laterally, highly variable shale content along bedding planes and geometric variability. Accordingly, GPR reflection characteristics and geometry for these horizons is very complex between E and · beds (Fig. 10b). Confident identification of the general location of these complex horizons between the E and · beds

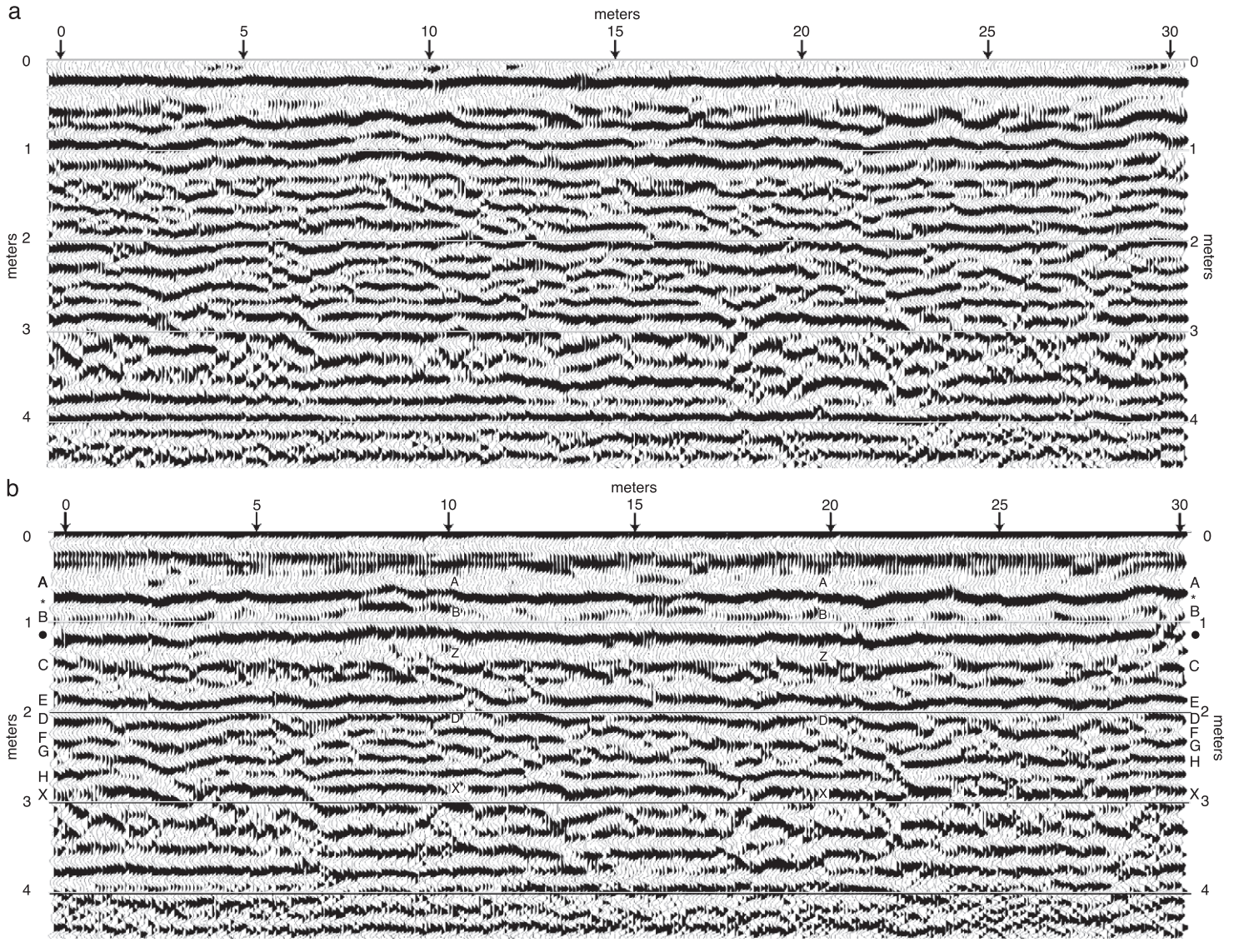

Fig. 10. (a) GPR data along a 30-m line on a flat bench 1 m behind quarry face BSG1 after trapezoidal bandpass filtering (80/130–400/500 MHz) and AGC (a 10-ns window) have been applied. (b) The same GPR data as shown in (a) after the deterministic deconvolution, the trapezoidal bandpass filtering and the AGC. Letters correspond to beds shown on Fig. 6.

provides the opportunity for further examination of the detailed associations of GPR reflection character and geology changes. In contrast, even speculative identification of just the general location of these complex bedded horizons between the E and · beds is virtually impossible on nondeconvolved data (Fig. 10a).

Deterministic deconvolution appears to enhance true amplitude of some reflections (e.g., Fig. 10b), which is consistent with stratigraphic/sedimentologic features on the quarry face (Fig. 6). For example, distinct and continuous beds * and · that contain consistent shale concentration at bedding planes on the quarry face are represented by reflections with higher amplitude and greater coherence. In contrast, beds A and B, characterized by lateral variations in shale concentration at bedding planes, are represented by reflections with lower amplitudes and less continuity. The GPR images of these beds are verified by the detailed examination and measurements on the quarry face, including 10 steel rod tests.

The comparisons we have used in this paper illustrate the effectiveness of the deterministic deconvolution in improving resolution and providing a more accurate spatial representation of geologic features. This processing step significantly aids interpretation and provides the opportunity for more detailed analyses of complex GPR reflections and the properties controlling GPR attributes.

6. Conclusions

This study provides an example of how deterministic deconvolution can increase resolution of GPR data. Keys to our success were the capturing of the GPR source wavelet, the use of conductive rods as markers and access to multiple clean quarry exposures. Our study indicates that source wavelet interference in GPR data can be markedly suppressed using deterministic deconvolution.

GPR source wavelets acquired in air (in an open outdoor setting devoid of natural and artificial noise) for the 400-MHz antennas (0.3-m spacing) possess well-behaved spectral properties. Wavelets from antennas will vary slightly from one instrument to the other, but once a wavelet is acquired and defined for a particular antenna, it can be permanently stored and used for all geologic settings and applications. Since wavelets acquired in air are true source wavelets, changes in the geologic material being imaged or coupled to will have no impact on the effectiveness of deterministic deconvolution in which these uniquely determined source wavelets are used.

The convolution model was verified by the deterministic deconvolution of GPR data acquired at a field study site characterized by carbonate strata interbedded with thin shale seams. Ultimate quantification of resolution and spatial accuracy of processed GPR data was obtained by inserting conductive steel rods into holes drilled horizontally into quarry faces. Verification studies confirmed data processed using deterministic deconvolution were far superior in all aspects over nondeconvolved GPR data. Applying deterministic deconvolution to GPR data collected in sedimentary strata at our study site resulted in improved resolution (50%) and improved spatial location (0.10–0.15 m) of geologic features compared to the same data processed without deterministic deconvolution. Results of our initial study indicate deterministic deconvolution can be successfully applied to reduce ringing in GPR studies of low dielectric loss material, such as the lithified carbonate strata of our study.

Acknowledgements

We thank Shawnee Rock, Bonner Springs, KS, especially Frank Rockers and Owen Crome, for kindly providing access to the quarry study site, cooperating in design of the project, and assistance during data acquisition. We thank Joe Anderson for the horizontal drilling and Choon Park for valuable discussion during data processing. We would like to thank Peter Annan and Milton Porsani for their critical and constructive review. We appreciate discussion with S.A. Arcone on the concept of the deterministic deconvolution. We also thank Mary Brohammer and Julia Shuklaper for assistance in preparation of this manuscript. This study was funded by the National Science Foundation (EAR 9912062) and the Kansas Geological Survey.

References

Annan, A.P., 1996. Ground Penetrating Radar (Workshop Notes). Sensors and Software, Canada.

Arcone, S.A., Lawson, D.E., Delaney, A.J., Strasser, J.C., Strasser, J.D., 1998. Ground-penetrating radar reflection profiling of groundwater and bedrock in an area of discontinuous permafrost. Geophysics 63, 1573–1584.

Butler, J., Franseen, E., Xia, J., Schulmeister, M., Zheng, L., Weis, T., Byrnes, A., Healey, J., Miller, R., 2000. Experimental assessments of the utility of direct-push profiling and ground-penetrating radar for hydrostratigraphic investigations. SEPM/IAS Research Conference Environmental Sedimentology Hydrogeology of Sedimentary Aquifers, Santa Fe, NM, September, 24–27. The International Association of Sedimentologists, pp. 26–27.

Claerbout, J.F., 1992. Earth Soundings Analysis: Processing Versus Inversion. Blackwell, Boston. 304 pp.

Franseen, E.K., Xia, J., Byrnes, A.P., Miller, R., Weis, T., Washburn, E., 2001. Controls on ground-penetrating radar reflections in Pennsylvanian carbonate strata: implications for processing and attribute analysis. Kansas Geological Survey Open-File Report 58, 51 pp.

Gottsche, F.M., Stolte, C., Nick, K.P., 1994. Two-sided deconvolution: a method to improve the temporal resolution in radar data. Extended Abstracts of 56th Meeting of European Association of Exploration Geophysicists, p. P049.

Knoll, M.D., 1996. A petrophysical basis for ground-penetrating radar and very early time electromagnetics, electrical properties of sand–clay mixture. Unpublished PhD dissertation, University of British Columbia. 316 pp.

Martinez, A.D., Byrnes, A.P., 2001. Modeling dielectric constant values of geologic materials: an aid to ground-penetrating radar data collection and interpretation. Current Research in Earth Sciences, Kansas Geological Survey Bulletin 247, part 1. http://www.kgs.ukans.edu/Current/2001/martinez/martinez1.html.

McKirahan, J., Goldstein, R.H., Franseen, E.K., 2000. Sequence stratigraphy of the Lane-Island Creek shales and the Farley limestone in Northeastern Kansas and geologic factors affecting the quality of limestone aggregates. K-TRAN Report no. KU-97-1. 236 pp.

Moran, M.L., Greenfield, R.J., Arcone, S.A., Delaney, A.J., 2000. Delineation of a complexly dipping temperate glacier bed using short-pulse radar arrays. Journal of Glaciology 46, 274–286.

Neves, F.A., Roulston, M.S., Miller, J.A., 1995. Source signature deconvolution of ground penetration radar data. Revista Brasileira de Geofisica 13 (2), 143–153.

Porsani, M.J., Ursin, B., 1996. Mixed-phase deconvolution of seismic and ground-penetrating radar data. Annual Meeting Abstracts. Society of Exploration Geophysicists, Tulsa, OK, pp. 1603–1606.

Todoeschuck, J.P., LaFlèche, P.T., Jensen, O.G., Judge, A.S., Pilon, J.A., 1992. Deconvolution of ground probing radar data. In: Pilon, J. (Ed.), Ground Penetrating Radar. Geological Survey of Canada, Paper 90-4, pp. 227–230.

Turner, G., 1992. Propagation deconvolution. In: Hanninen, P., Autio, S. (Eds.), Fourth International Conference on Ground Penetrating Radar. Geological Survey of Finland, pp. 85–93.

Turner, G., 1994. Subsurface radar propagation deconvolution. Geophysics 59, 215–223.

Xia, J., Weis, T., Franseen, E., Miller, R., 2001. Ground truth of ground-penetrating radar data at a limestone quarry. Presented at SAGEEP 2001 Annual Meeting of Environmental and Engineering Geophysical Society, March 4–7, 2001, Denver, CO. 12 pp.

Yilmaz, Ö., 1987. Seismic Data Processing. Society of Exploration Geophysicists, Tulsa, OK. 526 pp.